Mikrochim. Acta 117, 39–47 (1994)

Mikrochimica
Acta

Energy Filtered Transmission Electron Microscopy for the Physico-Chemical Characterization of Aquatic Submicron Colloids

Denis Mavrocordatos, Charles-Philippe Lienemann, and Didier Perret*

Institute de Chimie Minérale et Analytique, Université de Lausanne, BCH, CH-1015 Lausanne, Switzerland

Abstract. A combination of energy filtered transmission electron microscopic (EF-TEM) procedures is proposed for the non-perturbing physico-chemical characterization of submicron mineral and organic colloids in aquatic systems. Synthetic hematite microparticles and xanthan polysaccharides were used as well-characterized model colloids in order to determine the optimum EF-TEM analysis conditions. In this paper, it is demonstrated that (*i*) our model colloids are morphologically representative of naturally occurring mineral/organic associations, (*ii*) EF-TEM allows the detection of fine xanthan ultrastructures without artefacts of conventional staining methods and (*iii*) submicron hematite particles can be specifically visualized and spectrometrically measured by EF-TEM within a hematite/xanthan mixture. This EF-TEM procedure appears to be appropriate for the characterization of real aquatic samples.

Key words: hematite, xanthan, energy filtered transmission electron microscopy (EF-TEM), contrast tuning (CT), electron spectroscopic imaging (ESI), electron energy loss spectrometry (EELS).

Submicron autochthonous and weathered mineral colloids (iron oxyhydroxides, manganese oxides, silica, clays, aluminum oxides) are ubiquitous in freshwater systems [1, 2]. Despite their relatively low mass concentrations (typically < 5–10% of the total mass of mineral particles), these colloids have been shown to contribute an important proportion of the total particle numbers in natural waters [3, 4]; as a consequence of their high specific surface area, they are thus able to represent a large fraction of the total available surface of suspended solids.

Field studies have shown that submicron colloids may also be associated with pedogenic and aquogenic organic macromolecules (humics, polysaccharides)

---

* To whom correspondence should be addressed

[5, 6]. On the other hand, these colloids, and in particular amorphous iron-rich species, have been shown to act as powerful trace metal scavengers [7, 8]; strong microparticle/macromolecule interactions could explain discrepancies between field measurements and adsorption/surface complexation models derived from laboratory studies [9].

It is thus of utmost importance to develop sound analytical methodologies for the physico-chemical characterization of these submicron mineral and organic colloids, in order to improve realistic predictive models on the behavior of toxic trace metals in aquatic environments. Used in conjunction with appropriate sample fractionation and multi-method analysis schemes, electron microscopic techniques are powerful complementary tools, which allow the determination of morphological, elemental and even crystallographic data on the scale of the individual particles [4, 9, 10].

This field of interest has motivated us to design a scheme based on energy filtered transmission electron microscopy (EF-TEM) for the characterization of submicron mineral particles and their associated organic macromolecules. EF-TEM techniques have already found applications in biology and material science, but, to our knowledge, have been only rarely used in environmental science [11–13]. In order to mimic naturally occurring mineral and organic colloids and determine optimum analytical conditions, well-characterized hematite microparticles (α-Fe_2O_3) and polysaccharides (xanthan) were used.

Experimental

Materials and Model Colloids

Chemicals for the preparation of suspensions were *pro analysis* (Fluka), unless otherwise stated. Only ultrapure ultrafiltered UV-irradiated water was used (Elgastat UHQ-II). Manipulations were made at a laminar flow bench (Skan VFC 120) whenever possible, in order to avoid contamination by particles from the atmosphere.

Hematite microparticles were synthesized according to variations of procedures already described [14, 15]. A $3.5 \times 10^{-2} M$ solution of $Fe(ClO_4)_3$ (pract. 97%) in $5 \times 10^{-2} M$ $HClO_4$ was boiled for 24 h; microparticles produced by forced hydrolysis were purified by three ultracentrifugation steps ($RCF_{max} = 10^5$ g, 15 min; Centrikon T2070, swing-out rotor TST-28) into fresh $10^{-3} M$ $HClO_4$.

Monodisperse microparticles of 70 ± 5 nm were obtained as a stock suspension (ca. 2 g/l). XRD identification (Philips PW 1730/1710) revealed purely crystallized α-Fe_2O_3. Iron concentrations in the suspensions were measured by ICP-AES (Perkin-Elmer plasma 1000; $\lambda Fe = 208.204$ nm) after digestion of the particles in 5% HNO_3 and 0.1 M $H_2NOH \cdot HCl$ (100°C, 24 h).

Xanthan (MW $\approx 2 \times 10^6$ dalton; repeating units of D-glucose with a side-chain composed of D-glucuronic acid and D-mannose containing an acetyl and a pyruvate group) was obtained as a biopolymer concentrated gel produced by *Pseudomonas campestris* (Flocon 4800C; Pfizer, NY). Diluted suspensions of this polysaccharide (ca. 0.2 g/l) were prepared in $10^{-3} M$ $HClO_4$ and stirred for 24 h prior to use; fresh preparation avoided coalescence of the fibrils [16].

Working mixtures of hematite (0.3 mg/l) and xanthan (0.2 mg/l) were freshly prepared (5 min stirring, 24 h reaction). In order to enhance their contrast under the TEM, xanthan fibrils were lightly stained *en bloc* by adding an aliquot of a pre-filtered 2% uranyl acetate solution to the hematite/xanthan mixtures just before specimen preparation; final stain concentration in the samples was 0.1%.

Specimens for TEM and EF-TEM were prepared according to non-perturbing procedures described elsewhere [17, 18]; schematically, mixtures of hematite/xanthan were ultracentrifuged ($RCF_{max} = 5 \times 10^4$ g, 15 min; 4 ml mixture) in tubes containing TEM grids (Cu^0 200 mesh, collodion-covered, carbon-coated) which were recovered at the issue of the centrifugation and occasionally post-protected with an hydrophilic embedding resin (Nanoplast FB101) [19] prior to visualization.

Electron microscopy observations were done on a medium resolution TEM (Zeiss EM10; 80 keV) and on a high resolution EF-TEM (Zeiss CEM902 with a Castaing-Henry filter; 80 keV) for Contrast Tuning (CT), Electron Spectroscopic Imaging (ESI) and Electron Energy Loss Spectrometry (EELS) modes.

EF-TEM Methodology

Conventional TEM (CTEM) does not give any information on the elemental composition of each component present in a specimen under study. The EF-TEM can address this lack by taking advantage of the different electron–matter processes that give rise to an image. Amongst others, incident electrons of the beam can undergo elastic and inelastic shocks with the irradiated matter; while the former induce no loss of energy to the scattered electrons, the latter are the source of information we need because the loss of energy of scattered electrons depends directly on the nature of the irradiated compounds [20]. Figure 1 gives a summary of the most interesting features and analysis modes of an EF-TEM.

On an EF-TEM, the electromagnetic prism present under the specimen acts like a grating in a conventional photon spectrometer; it allows filtering of the different electrons that have interacted with the specimen as a function of their energy. In contrast to a CTEM, which produces images on a fluorescent screen resulting from all elastic and inelastic scattering processes, an EF-TEM filters out all electrons except those which have lost a discrete amount of energy (ΔE_{loss} between 0 and ca. 2000 eV).

In practice, the prism is held in a fixed position and the energy of the incident beam (E_0; nominal accelerating voltage) is increased by ΔE_{loss}, so that the detector (fluorescent screen, TV

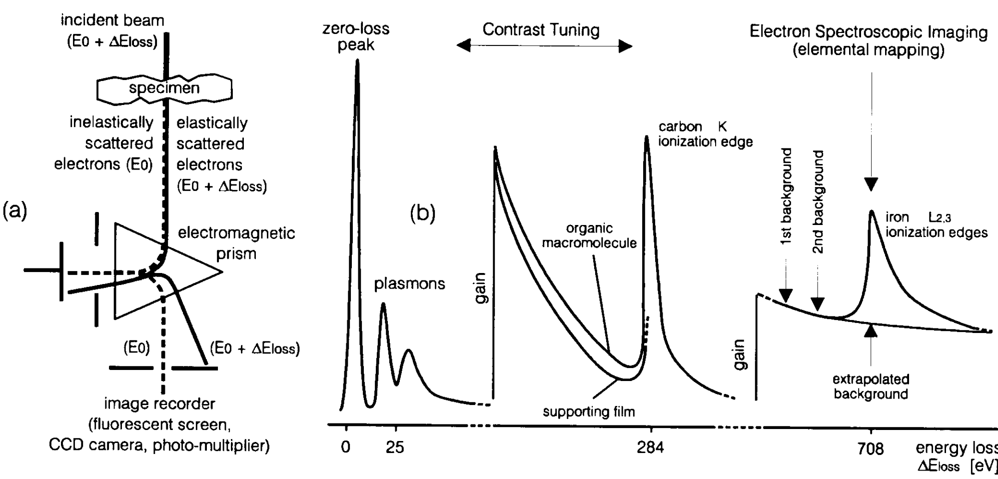

Fig. 1. **a** Schematic diagram of an EF-TEM. **b** EELS spectrum of an ideal specimen. The zero-loss peak refers to elastically scattered electrons only; the contrast tuning region shows the difference in recorded intensities between a poorly electron-dense material (organic matter) and the background (carbon supporting film); electron spectroscopic imaging (elemental mapping) is obtained by a subtracting algorithm, images recorded below the ionization edge allowing background extrapolation

camera or photo-multiplier) always records the same electron energy (E_0; 80 keV in our case). The different measuring modes which can be utilized in the characterization of envrionmental colloids are described below.

Zero-Loss and Contrast Tuning of Organic Macromolecules

Visualizing exclusively unscattered and elastically scattered electrons (energy filtering with $\Delta E_{loss} = 0$ eV; Fig. 1) eliminates inelastically scattered electrons that contribute to chromatic aberration and decrease the final contrast of the image. This method is known as zero-loss imaging [21], and produces images on a fluorescent screen with a higher resolution and higher contrast than CTEM, especially for biological specimens, which usually contain only a few electron-dense elements.

The K ionization edge of carbon atoms appears at $\Delta E_{loss} = 284$ eV; the energy loss region below this edge is known as the contrast tuning region where differences in signal intensities between a carbon supporting film and an organic specimen (containing elements with $Z > 6$) give rise to distinct shapes of ΔE_{loss} curves (Fig. 1). For most biological specimens, the highest contrast is obtained close to $\Delta E_{loss} = 250$ eV (structure-sensitive contrast) [22], but the accurate energy value at which the image will be visualized with the highest contrast on the fluorescent screen has to be empirically determined, depending on the composition of the specimen.

Electron Spectroscopic Imaging and Electron Energy Loss Spectrometry of Mineral Microparticles

The complete spectrum (intensity vs. ΔE_{loss}) which can be recorded by a photo-multiplier tube when varying ΔE_{loss} at the incident electrons (Fig. 1) is characteristic of the elements present in the analysed specimen, with ionization edges of the elements appearing at discrete energy losses. This measuring mode is known as electron energy loss spectrometry, and relative or absolute quantification can be done on a spectrum, for virtually every element ($Z = 3$–92), provided the specimen thickness fulfills certain conditions [20].

Electron spectroscopic imaging is an interesting vizualization mode, where the image, obtained on a TV camera, is representative of the analysed element (i.e. at the ionization edge of the element), without contributions from the background. The elemental image is obtained by the following algorithm [22] (Fig. 1): (*i*) two images are recorded below the ionization edge of the element, (*ii*) from these two images, an extrapolated background image is calculated at the ionization edge, (*iii*) this extrapolated image is electronically subtracted from the image recorded at the ionization edge, thus resulting in a map distribution of the element determined in the specimen.

Results and Discussion

Figure 2 shows a comparison between a natural sample and a synthetic mixture of hematite and xanthan. From a morphological point of view, organic matter in this natural sample is probably polysaccharidic and is usually present as isolated or networked fibrils, either connected to the producing biota (algae, bacteria) or detached from them [6].

Organic matter in aquatic specimens appears as poorly electron-dense material being naturally stained by inorganic ions present in the natural waters; however, many organic entities usually appear as weakly contrasted objects, even under drastic imaging conditions (small TEM objective aperture, contrast enhancement during the printing process). As shown in Fig. 2, submicron mineral

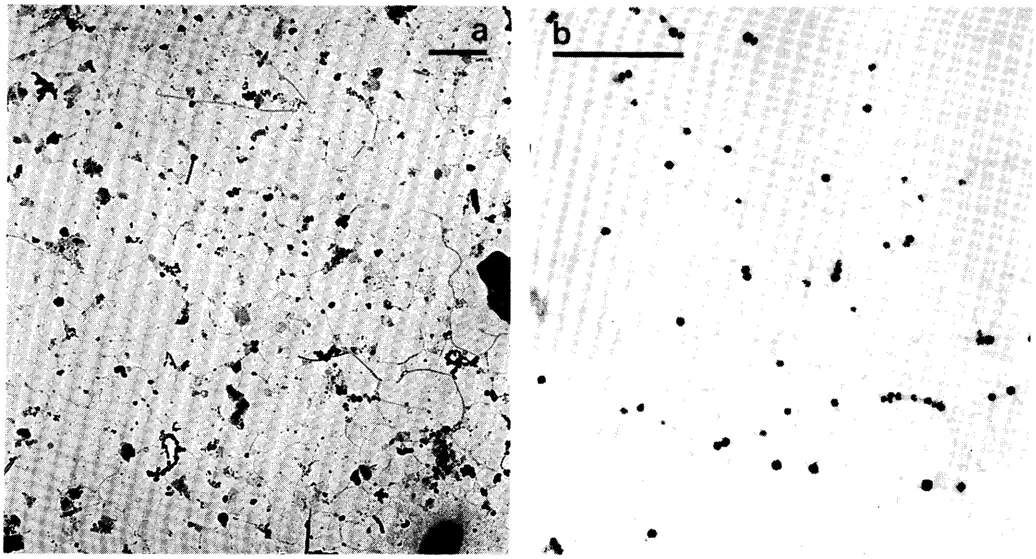

Fig. 2. **a** CTEM of a natural sample (River Rhine; supernatant of a pre-centrifuged sample) containing ca. 5 mg/l total particulates and ca. 2 mg/l organic matter. **b** CTEM of a mildly stained (uranyl acetate 0.1%, *en bloc*) mixture of hematite (0.3 mg/l) and xanthan (0.2 mg/l), showing the morphological similarities in microparticle/macromolecule interactions between a real aquatic suspension and a synthetic model. Scale bar: 1 μm

particles are commonly attached to these fibrils, probably indicating that the latter are able to stabilize microparticles, at least momentarily.

Similarly, synthetic hematite/xanthan mixtures ([α-Fe_2O_3)]/[xanthan] = 0.5–10) form large-scale entities, where polysaccharides are grouped into loose networks at the surface of which hematite microparticles are always attached. It is necessary to stain these synthetic mixtures under mild conditions in order to allow visualization of xanthan by CTEM; 0.1% uranyl acetate *en bloc* staining proved to generate an optimum contrast. Coalescence of the fibrils and precipitation/denaturation of the specimen at high stain concentration or during classical post-staining procedures [23] could thus be avoided.

It was checked that post-protection of specimens with a hydrophilic resin (i.e. surface coverage of specimen after deposition on TEM grid) was neither perturbing nor compulsory for our synthetic mixtures; however, this step is necessary for fragile structures and colloids influenced by redox conditions (i.e. samples from anoxic waters), as observed from environmental samples [10, 18] and preliminary syntheses of amorphous iron oxyhydroxides under slightly oxic conditions.

Figure 3 shows a hematite/xanthan mixture prepared in the conditions given above, and analysed by CTEM at the ultrastructural level, zero-loss imaging, contrast tuning and electron spectroscopic imaging. CTEM of lightly stained (0.1% uranyl acetate) xanthan at high magnification (Fig. 3a) reveals fibrils with diameter > 8 nm, in agreement with other observations (platinum rotary shadowing of fibrils) [24]; their apparent structure is not smooth, mainly because low stain concentration does not uniformly contrast the macromolecular structure. As a

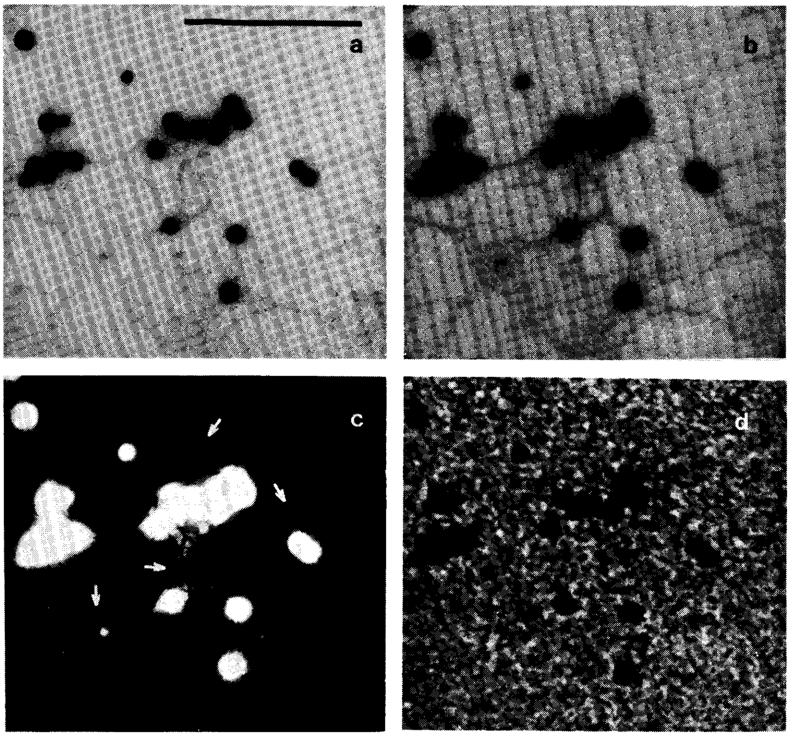

Fig. 3. **a** High magnification CTEM of a [hematite]/[xanthan] = 1.5 (w/w) mixture (uranyl acetate 0.1%, *en bloc*). **b** Same specimen, in zero-loss imaging ($\Delta E_{loss} = 0\,eV$, resolution window $\delta E_{loss} = 17\,eV$). **c** Same specimen, in contrast tuning mode ($\Delta E_{loss} = 250\,eV$, $\delta E_{loss} = 17\,eV$). **d** Same specimen, in electron spectroscopic imaging (map distribution of individual iron microparticles; Fe $L_{2,3}$ edge at $\Delta E_{loss} = 716\,eV$, $\delta E_{loss} = 13\,eV$). Scale bar: 1 µm

consequence, ultrathin fibrils radiating out of the main framework of fibrils cannot be visualized. A higher staining effect can be obtained (> 0.1% uranyl acetate), but at the expense of an alteration of the original fibrils structure within the framework or a coalescence of smaller entities into thicker fibrils (15–20 nm).

Zero-loss imaging (Fig. 3b) enhances the total contrast of particles and fibrils, but, as for CTEM, finer details are not revealed and the structure of visible fibrils still appears as ill-defined. A more interesting result is obtained when only inelastically scattered electrons at $\Delta E_{loss} = 250\,eV$ are visualized (Fig. 3c). As previously mentioned, determination of the optimum ΔE_{loss} in contrast tuning mode depends on the composition of the specimen. In our case, visualizations at ΔE_{loss} between 30 and 250 eV produce an increase in contrast on xanthan fibrils. Optimum ultrastructural information is achieved at 250 eV, which is in agreement with results usually obtained on resin-embedded biological samples.

High contrasting of poorly electron-dense fibrils is illustrated by the fact that ultrathin fibrils (5–7 nm, arrowed on Fig. 3c) are revealed with this technique while obscured by CTEM and zero-loss imaging. Thicker entities are also sharply recorded, resulting in a high image resolution of coalesced fibrils and nodes. Contrast tuning mode allows a better visualization of the associations between macromolecular fibrils and particles, showing ultrastructural details on the morphology of organic material surrounding hematite microparticles and in the fibrils network.

Provided specimen thickness is within the optimum analytical range (< ca. 200 nm), elemental mapping obtained by electron spectroscopic imaging distinctly produces information on the composition of the specimen. Figure 3 d shows the elemental image of iron present in the synthetic hematite/xanthan mixture. With the resolution window used in ESI mode ($\delta E_{loss} = 13$ eV), Fe L_3 ($\Delta E_{loss} = 708$ eV) and Fe L_2 ($\Delta E_{loss} = 721$ eV) ionization edges are not discriminated and show a maximum at $\Delta E_{loss} = 716$ eV (Fe $L_{2,3}$). The Fe pre-edge (680 eV, 690 eV) was used for background extrapolation at 716 eV, and the final image obtained at this value of ΔE_{loss} has been recalculated after extrapolated background subtraction. The primary magnification used for this image (30000 ×) allows the recording of elemental information over a large area, where elements other than iron are spectroscopically excluded. The signal intensity of each pixel in the ESI image is proportional to the quantity of the measured element, and further image analysis could provide relative quantification of the latter.

Actually, it is possible to characterize hematite microparticles by electron energy loss spectrometry under the experimental conditions used in material science for thin evaporated films or etched specimens. The spectrum of Fig. 4 has been obtained on one of the hematite microparticles present in Fig. 3, and clearly exhibits the oxygen K edge (537 eV) and the iron L_3 and L_2 edges (respectively 708 and 721 eV). Acquisition of the spectrum at high magnification (85000 ×) with a high resolution ($\delta E_{loss} = 2$ eV) and the use of a small pre-filter aperture (10 μm) allow the analysed microparticle to be completely covered by the incident beam, thus increasing the signal/noise ratio by reducing non-specific electrons reaching the filter.

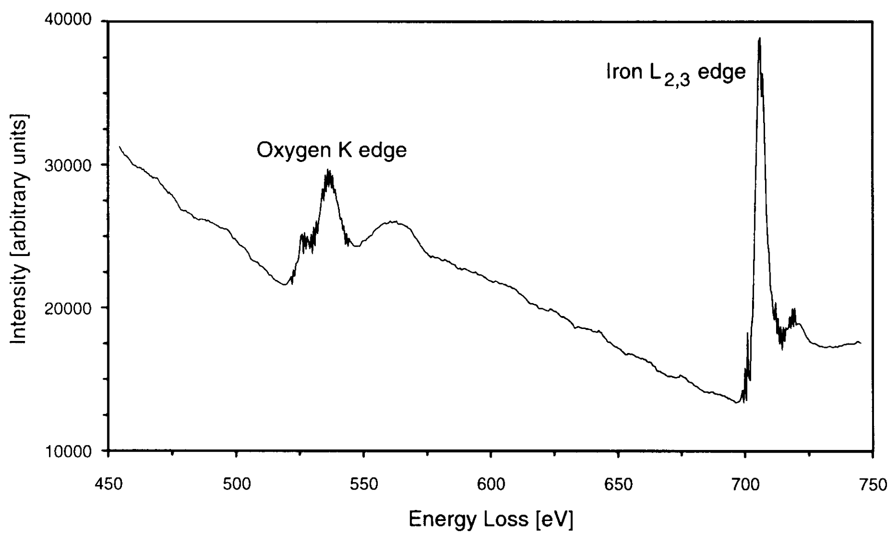

Fig. 4. Electron energy loss spectrum of one of the submicron hematite particles of Figure 3, showing oxygen K and iron L_3 and L_2 edges. Primary magnification = 85000 ×, scan rate = 1 eV/s, scan step = 0.5 eV, $\delta E_{loss} = 2$ eV, collection angle > 80 mrad. This spectrum has undergone a smoothing algorithm in order to reduce background noise

Electron energy loss spectrometry is usually applied to homogeneously thin material (typically 10–30 nm); this procedure has the advantage of avoiding multi-scattering induced by thick specimens (ca. > 200 nm). With our specimen preparation procedure dedicated to natural or model colloids, we try however to maintain as far as possible the native state of the samples; therefore, the thickness of each individual particle cannot be controlled. Hopefully, model hematite microparticles are monodisperse, and our results show that they can be analysed by EELS without further problems, excluding drift of the specimen during spectrum acquisition. From our preliminary investigations, the actual thickness range of iron oxide which can be analysed by EELS is between 50 and 150 nm. Compared with other analytical electron microscopies, like energy dispersive spectrometry (EDS-TEM) [25], there is actually no accurate EELS database on the elemental characterization of individual mineral particles smaller than ca. 100 nm; we have however the potential to address this database deficiency with the procedures described above.

Conclusions

Synthetic mixtures of submicron hematite particles and high molecular weight xanthan reveal strong interactions between mineral and organic components, thus making these mixtures an ideal model for the study of microparticle/polysaccharide entities evidenced in riverine and lacustrine waters [4, 26]. In order to visualize these macro-associations by CTEM on a *per particle* basis without denaturation, direct staining of organic macromolecules *en bloc* under mild conditions is advised.

EF-TEM in zero-loss imaging ($\Delta E_{\mathrm{loss}} = 0\,\mathrm{eV}$), but even better in contrast tuning mode below the carbon K edge ($\Delta E_{\mathrm{loss}} = 250\,\mathrm{eV}$), has proved to be a powerful technique for the characterization of organic fibrils; this method circumvents the need for high concentrations of heavy metal stains and reveals contact interactions between individual hematite microparticles and xanthan fibrils at the ultrastructural level with high resolution and contrast, as opposed to CTEM. Mild staining with 0.1% uranyl acetate and contrast enhancement by contrast tuning allow analysis of fragile ultrathin organic entities which were ignored until now by conventional techniques.

The use of EF-TEM in electron spectroscopic imaging mode allows the very specific identification of iron present in hematite microparticles, calculated $\mathrm{Fe}\,L_{2,3}$ images being obtained for an actual thickness of ca. 70 nm. On the other hand, the elemental composition of individual submicron hematite particles is obtained by EF-TEM in EELS mode. It is expected from electron energy loss spectra that iron-rich microparticles in the size range 5–150 nm might be measurable by this technique [27].

The EF-TEM procedures allow us to avoid problems of inherent low contrast encountered when studying fine organic ultrastructures under the microscope and to overcome individual particle size limitations (ca. > 50–100 nm) imposed by conventional EDS-TEM. Further extensions of EF-TEM to submicron mineral colloids containing aluminum (aluminum oxides), silicon (silica), mixtures of them (clays) or manganese (manganese oxides) should prove highly valuable for the physico-chemical characterization of individual microparticles and their role in natural aquatic systems.

Acknowledgements. We are grateful to Prof. G. G. Leppard (McMaster University, Hamilton; Ontario) for his critical reviewing and fruitful discussions, and to Dr. S. Dadras and F. Ardizzoni (Center of Electron Microscopy; University of Lausanne) for their help on electron microscopes. This work was supported by grants from the Swiss National Science Foundation (project 21-36593.92) and from the Agassiz Foundation.

References

[1] T. Nomizu, T. Nozue, A. Mizuike, *Mikrochim. Acta* **1987**, *II*, 99.
[2] T. F. Rees, J. F. Ranville, *J. Contam. Hydrol.* **1990**, *6*, 241.
[3] J. Buffle, H. P. Van Leeuwen (eds.), *Environmental Particles I*, Lewis, Chelsea, 1992.
[4] D. Perret, M. E. Newman, J.-C. Nègre, Y. Chen, J. Buffle, *Water Res.***1994**, *28*, 91.
[5] T. Nomizu, J. Nagamine, A. Mizuike, *Mikrochim. Acta* **1989**, *III*, 69.
[6] G. G. Leppard, in: *Environmental Particles I* (J. Buffle, H. P. Van Leeuwen, eds.), Lewis, Chelsea, 1992, p. 231.
[7] L. Sigg, in: *Aquatic Surface Chemistry* (W. Stumm, ed.), Wiley-Interscience, New York, 1987, p. 319.
[8] J. A. Davis, D. B. Kent, in: *Mineral-Water Interface Geochemistry, Reviews in Mineralogy, Vol. 23*, (M. F. Hochella Jr., A. F. White, eds.), Mineralogical Society of America, Washington, 1991, p. 177.
[9] D. Fortin, G. G. Leppard, A. Tessier, *Geochim. Cosmochim. Acta* **1993**, *57*, 4391.
[10] G. G. Leppard, J. Buffle, R. R. De Vitre, D. Perret, *Arch. Hydrobiol.* **1988**, *113*, 405.
[11] M. T. Otten, B. Miner, J. H. Rask, P. R. Busek, *Ultramicroscopy* **1985**, *18*, 285.
[12] C. Xhoffer, P. Berghmans, I. Muir, W. Jacob, R. Van Grieken, F. Adams, *J. Microsc.* **1991**, *162*, 179.
[13] D. Bouchet, *Microsc. Microanal. Microstruct.* **1993**, *4*, 387.
[14] N. H. G. Penners, *The Preparation and Stability of Monodisperse Colloidal Haematite (α-Fe_2O_3)*, PhD Thesis, University of Wageningen, Wageningen, 1985.
[15] L. Liang, *Effects of Surface Chemistry on Kinetics of Coagulation of Submicron Iron Oxide Particles (α-Fe_2O_3) in Water*, PhD Thesis, Caltech, Pasadena, 1988.
[16] G. G. Leppard, A. Massalski, D. R. S. Lean, *Protoplasma* **1977**, *92*, 289.
[17] T. Nomizu, A. Mizuike, *Mikrochim. Acta* **1986**, *I*, 65.
[18] D. Perret, G. G. Leppard, M. Müller, N. Belzile. R. R. DeVitre, J. Buffle, *Water Res.* **1991**, *25*, 1333.
[19] D. Frösch, C. Westphal, *Electron. Microsc. Rev.* **1989**, *2*, 231.
[20] R. F. Egerton, *Electron Energy-Loss Spectroscopy in the Electron Miscroscope*, Plenum, NewYork, 1986.
[21] R. R. Schröder, *J. Microsc.* **1992**, *166*, 389.
[22] L. Reimer, I. Fromm, P. Hirsch, U. Plate, R. Rennekamp, *Ultramicroscopy* **1992**, *46*, 335.
[23] H. Fehrenbach, J. Richter, P. A. Schnabel, *J. Microsc.* **1992**, *166*, 401.
[24] B. T. Stokke, O. Smidsrod, A. Elgsaeter, *Biopolymers* **1989**, *28*, 617.
[25] G. G. Leppard, R. R. DeVitre, D. Perret, J. Buffle, *Sci. Tot. Environ.* **1989**, *87/88*, 345.
[26] J. Pizarro, N. Belzile, M. Filella, G. G. Leppard, J.-C. Nègre, D. Perret, J. Buffle, *Water Res.*, in press.
[27] S. B. Andrews, R. D. Leapman, *Europ. Microsc. Anal.* **1993**, *24*, 21

Received June 1, 1994. Revision July 8, 1994.